Chapter 4

Estimation of a velocity anomaly from field data

In this chapter the velocity estimation from beam-stacked data is applied to the problem of estimating a low-velocity anomaly from field data. The data set is particularly interesting for use in testing a velocity-estimation method, because the velocity anomaly is shorter than the cable's length and it is not located near the surface but is centered at a depth of about 1.6 km. Therefore both the lateral and the vertical resolution of the estimation method are tested by the problems presented by the data. The anomaly causes a pull-down of the reflections from the top of an anticline; this pull-down can be corrected only if a good velocity model is used as an input for depth migration. Furthermore, the anomaly causes non-hyperbolic moveouts in the reflections. The non-hyperbolicity of the moveouts can be measured by use of beam stack and should be predicted by the estimated velocity model.

4.1 ANALYSIS OF THE DATA SET

The data that I present in this chapter are part of a marine survey recorded in the Adriatic Sea and donated to SEP by AGIP (Harlan, 1989; Leger et al., 1989). The data were recorded with steam-gun sources and a 2.35-km cable. The shot spacing is 25 m and the group interval is 50 m; consequently the midpoint coverage is 48 fold and the midpoint spacing is 25 m. I sorted the data in common-midpoint gathers and kept the 341 gathers that were full-fold. The data were sampled every 2 ms and were wide-band in frequency; reflected energy was as high as 100 Hz. SEP received the data already gained and deconvolved; I then muted the data to eliminate the first arrivals and dip-filtered the constant-offset sections to remove some steeply dipping noise.

Figure 4.1 shows the stack of the data. A large pull-down is visible in the stacked section near the midpoint location of 5.5 km; this pull-down is the effect of a low-velocity zone caused by gas. The gas is contained in a few sand layers on the top of an anticline, in coincidence with the "bright spots" that are visible between 1 and 2 s in the stack.

The data set does not need to be migrated before stack, because the reflections underneath the anomaly stacked coherently, even if their moveouts were not hyperbolic. On the other hand, a post-stack depth migration and a good velocity model are needed to position correctly the reflectors. Depth migration is particularly needed for correctly positioning the top of the anticline, which has been flattened by the velocity anomaly. The conventional methods for estimating interval velocity from stacking velocities cannot be used for this data set because the anomaly's width, which is about 2 km, is smaller than length of the cable. Therefore this data set is a good test case for a tomographic velocity estimation method such as the one using beam stacks.

4.1.1 Effects of the anomaly on prestack data

The low-velocity anomaly can be estimated by a tomographic procedure from measurements of its effects on the moveouts of the reflections. The velocity estimation proposed in this thesis uses as data the measurements of the moveouts obtained by the beam stack. Therefore I will first examine the effects of the anomaly on the prestack data and on the beam-stacked data. The perturbations in the beam stacks' kinematics caused by the anomaly should be in qualitative agreement with the theory that I developed in the last chapters.

Figure 4.2 and Figure 4.3 show slices of the beam-stacked data cube. These figures show beam stacks' semblance as a function of offset and midpoint location for a constant offset ray parameter and following the reflections correspondent to two reflectors. Figure 4.2 shows the beam stack for the reflector at about 2 s in the stacked section and for p_h equal to 0.206 s/km. Figure 4.3 shows the beam stack for the reflector at about 3.1 s and p_h equal to 0.089 s/km. The effects of the anomaly are evident in both figures; the offsets of the semblance peaks are larger at the midpoint locations above the anomaly and lower on its sides. These perturbations are in agreement with the results of the model study of section 2.4. The perturbations are larger for the deeper reflector than for the shallower reflector because the effects of ray bending increase with depth, as predicted by the amplitudes of the back-projection operator derived in section 3.2.2.

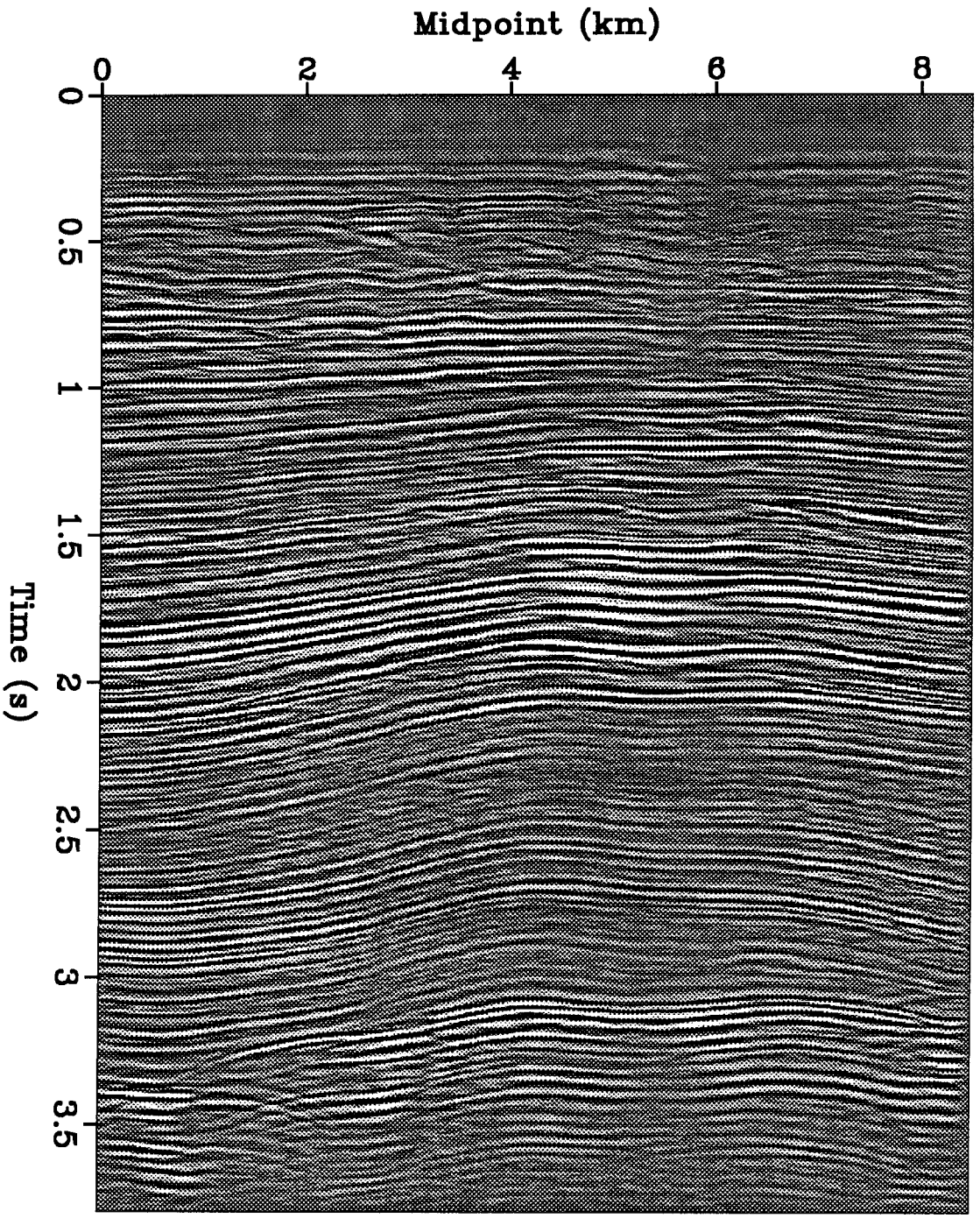

FIG. 4.1. The stacked section of the AGIP data set. A low velocity anomaly causes the time sag near the midpoint location of 5.5 km.

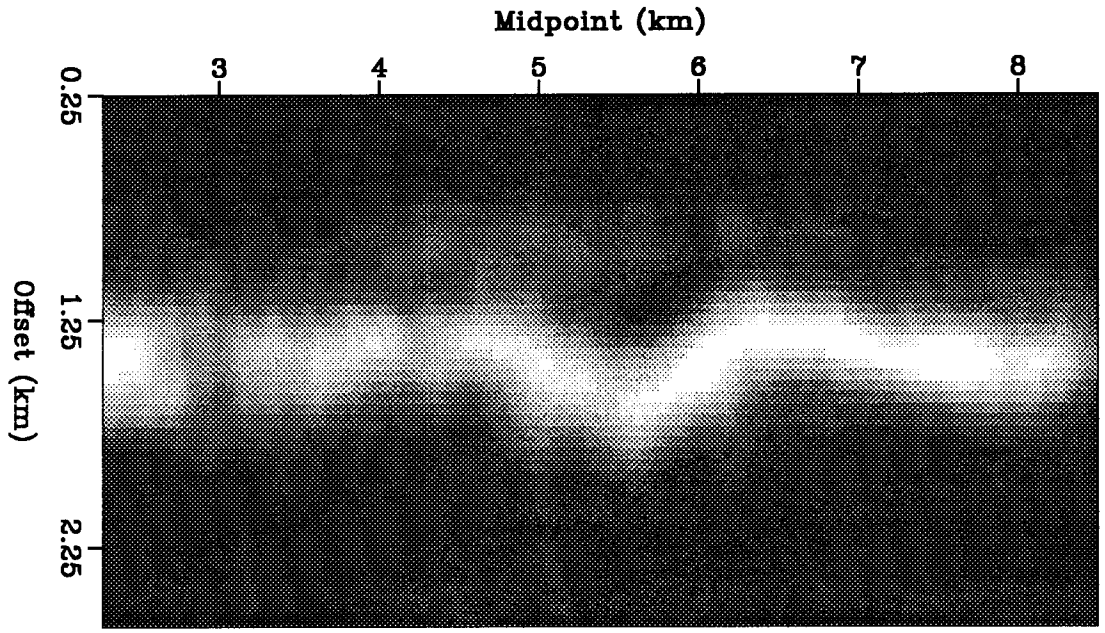

FIG. 4.2. The beam stacks' semblance as a function of offset and midpoint location, for the reflector at about 2 s in the stacked section of Figure 4.1. Beam stacks' offsets are larger at the midpoints located above the anomaly, and lower on its sides.

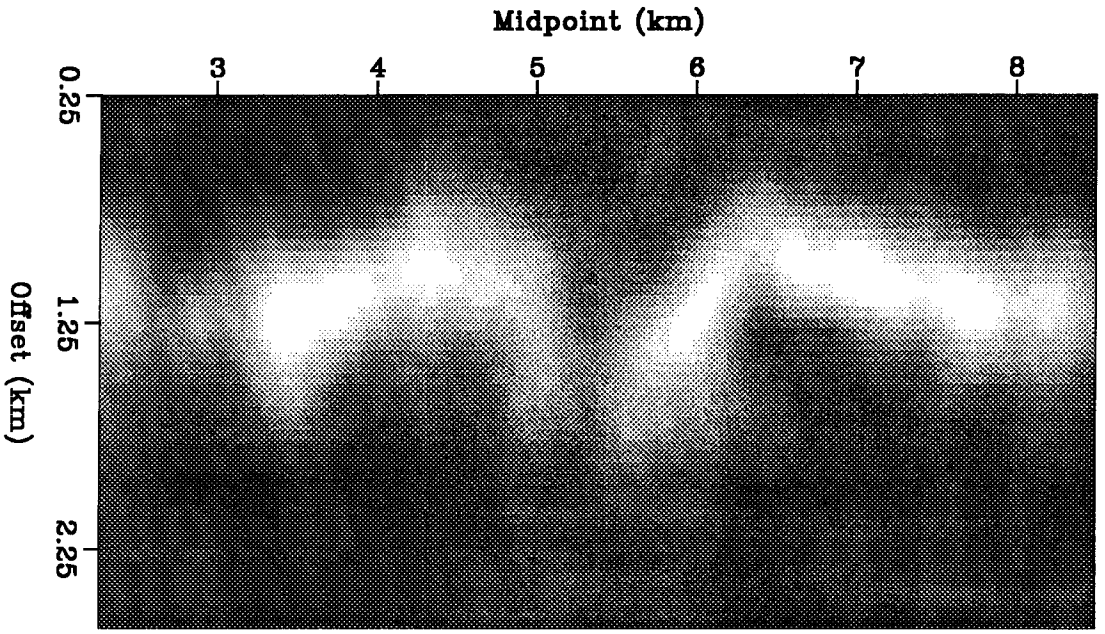

FIG. 4.3. The beam stacks' semblance as a function of offset and midpoint location, for the reflector at about 3.1 s in the stacked section of Figure 4.1. Beam stacks' offsets are larger at the midpoints located above the anomaly, and lower on its sides.

The velocity anomaly is localized enough to cause non-hyperbolic moveouts in the data. Beam stacks can measure these non-hyperbolic moveouts because they are local coherency operators. Figure 4.4 shows the effects of the anomaly on the reflections belonging to the CMP gather at location 6.45 km. The figure on the left shows a window of the data after the application of a hyperbolic normal moveout with velocity of 2.79 km/s. The figure on the right shows beam stacks' semblance as a function of offset and ray parameter for the reflection at 3.12 s. The black line superimposed onto the semblance plot shows what the offsets would be as a function of the ray parameter if the moveout were perfectly hyperbolic. The non-hyperbolicity of the moveouts is evident from the beam stacks. The anomaly has similar effects on the moveouts belonging to the CMP gather at location 4.8 km, that is on the other side of the anomaly with respect to the previous figure. A window of this gather, after the application of a hyperbolic normal moveout with velocity of 2.95 km/s, is shown on the left side of Figure 4.5. The figure on the right shows beam stacks' semblance as a function of offset and ray parameter for the reflection at 3.13 s. The black lines superimposed to the semblance plots show what the offsets would be as a function of the ray parameter if the moveouts were perfectly hyperbolic. For this CMP location the non-hyperbolicity of the moveouts is less evident than for the CMP gather shown in Figure 4.4. The non-hyperbolicity of the moveouts is more evident in the beam stacked-data than in the data shown in the usual time-offset domain.

4.2 THE ESTIMATION RESULTS

The first step of the estimation procedure described in Chapter 3 is the transformation of the prestack data by use of a two-dimensional beam stack (section 2.2.4). I computed beam stacks from the prestack data for 12 offset ray parameters p_h, from 0.05 s/km to 0.336 s/km, and for three midpoint ray parameters p_y, from -.04 s/km to .04 s/km. I transformed the beam-stacks according to the traveltime transformation introduced in Chapter 3 [equation (3.4)]. I then smoothed the transformed data along the midpoint axis and the time axis using Gaussian windows. The smoothed and transformed data from the 250 midpoint positions located around the anomaly were used by the velocity estimation.

The starting solution for the iterative estimation algorithm was a velocity profile function of depth, which was constant in the lateral direction. This velocity function was derived from conventional stacking-velocity analysis applied to a few of the CMP gathers. The velocity model was parametrized with B-spline functions, one basis function every

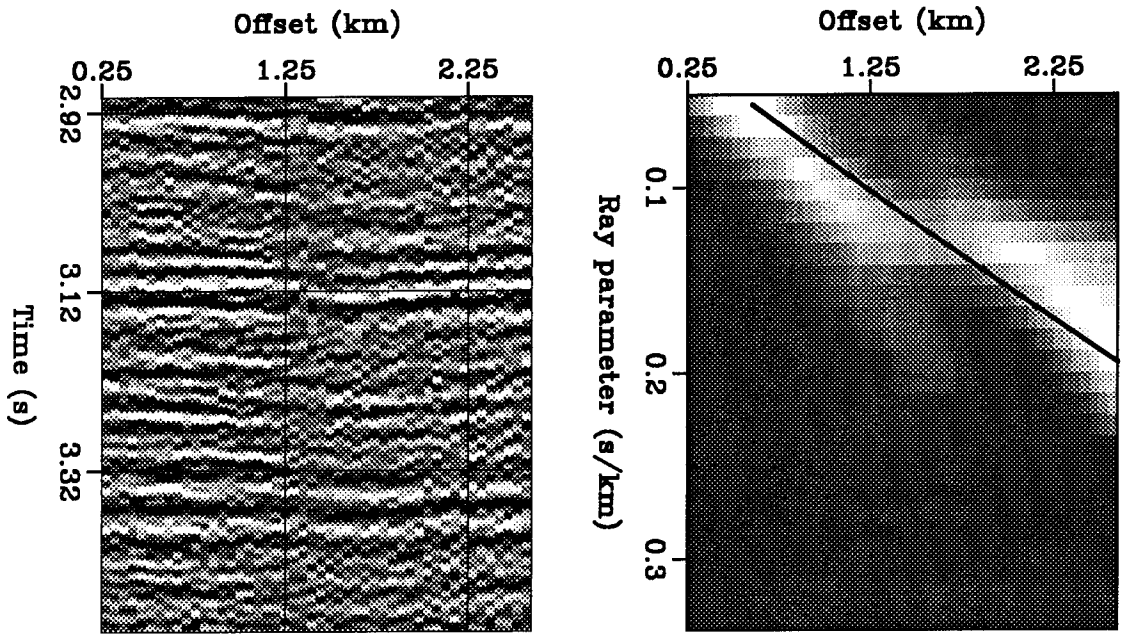

FIG. 4.4. A window of a CMP gather after hyperbolic moveout with velocity of 2.79 km/s has been applied (left), and the beam stack's semblance for the reflection at 3.12 s (right). The black line superimposed onto the semblance plot shows what the offsets would be as a function of the ray parameter if the moveout were perfectly hyperbolic.

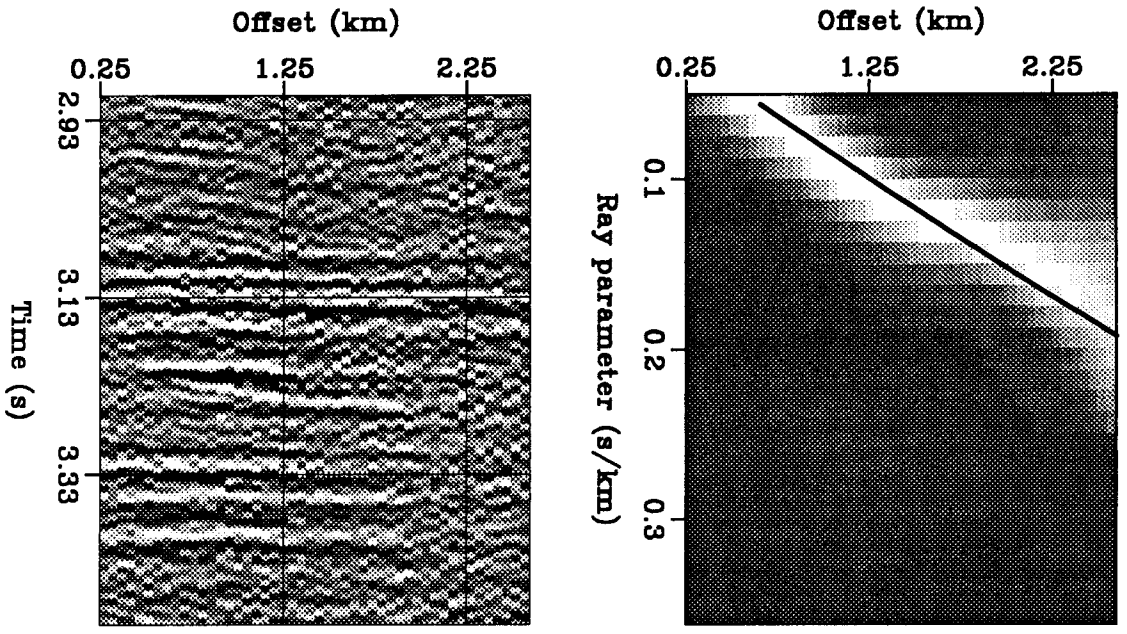

FIG. 4.5. A window of a CMP gather after hyperbolic moveout with velocity of 2.95 km/s has been applied (left), and the beam stack's semblance for the reflection at 3.13 s (right). The black line superimposed onto the semblance plot shows what the offsets would be as a function of the ray parameter if the moveout were perfectly hyperbolic.

500 m in the vertical direction and one every 1000 m in the horizontal direction. The estimation procedure started with a few conjugate gradient iterations until the velocity model predicted the gross feature of the beam-stacked data, and then continued with some Gauss-Newton iterations for better estimating the finer components of the velocity function. For the last iteration of the Gauss-Newton algorithm I increased the bandwidth of the model by reducing the horizontal spacing of B-spline functions to 800 m.

The result of the estimation process is a velocity model with a velocity anomaly located around the midpoint location at 5.5 kilometers and centered at a depth of 1.6 kilometers. Figure 4.6 shows the resulting velocity model as the sum of two components: one background velocity profile, which is a function of depth but is constant in the lateral direction, and one anomalous model, which is a function of both depth and the lateral position. The anomalous model is shown with a contour plot superimposed to the result of a migration of the stacked section using the estimated velocity. The contour interval is -40 m/s, and the maximum amplitude of the anomaly is about 230 m/s. The estimated velocity anomaly is correctly positioned in coincidence with the bright spots. The anomaly has a low lobe with anomalous velocity of about -50 m/s between the depths of 3 to 4 km. This low-lobe may correspond to a real feature of the velocity function or may be an artifact of the estimation; in this region the velocity is not well determined because of the absence of strong reflectors.

Figure 4.7 shows the result of migrating the stacked section with the background velocity. Migrating the stacked section with the background velocity as a velocity function did not correct the pull-down in the structure, although it approximately focused the data. Figure 4.8 shows the result of migrating the stacked section using as a velocity function the estimated velocity model; that is, the background plus the anomalous velocity model. The inclusion of the anomaly has caused a considerable change in the positioning of the reflectors.

The two migration results are better compared by a look at the windows of the data that have been directly affected by the anomaly, as shown in Figure 4.9. The estimated velocity field corrects the mispositioning of the top of the anticline, both laterally and in depth. Furthermore, the migration with the background velocity did not perfectly focus the deeper reflectors; this misfocusing caused a decrease in the amplitudes of the migrated reflectors underneath the anomaly. This focusing effect is corrected in the migration that used the estimated velocity model as a velocity function.

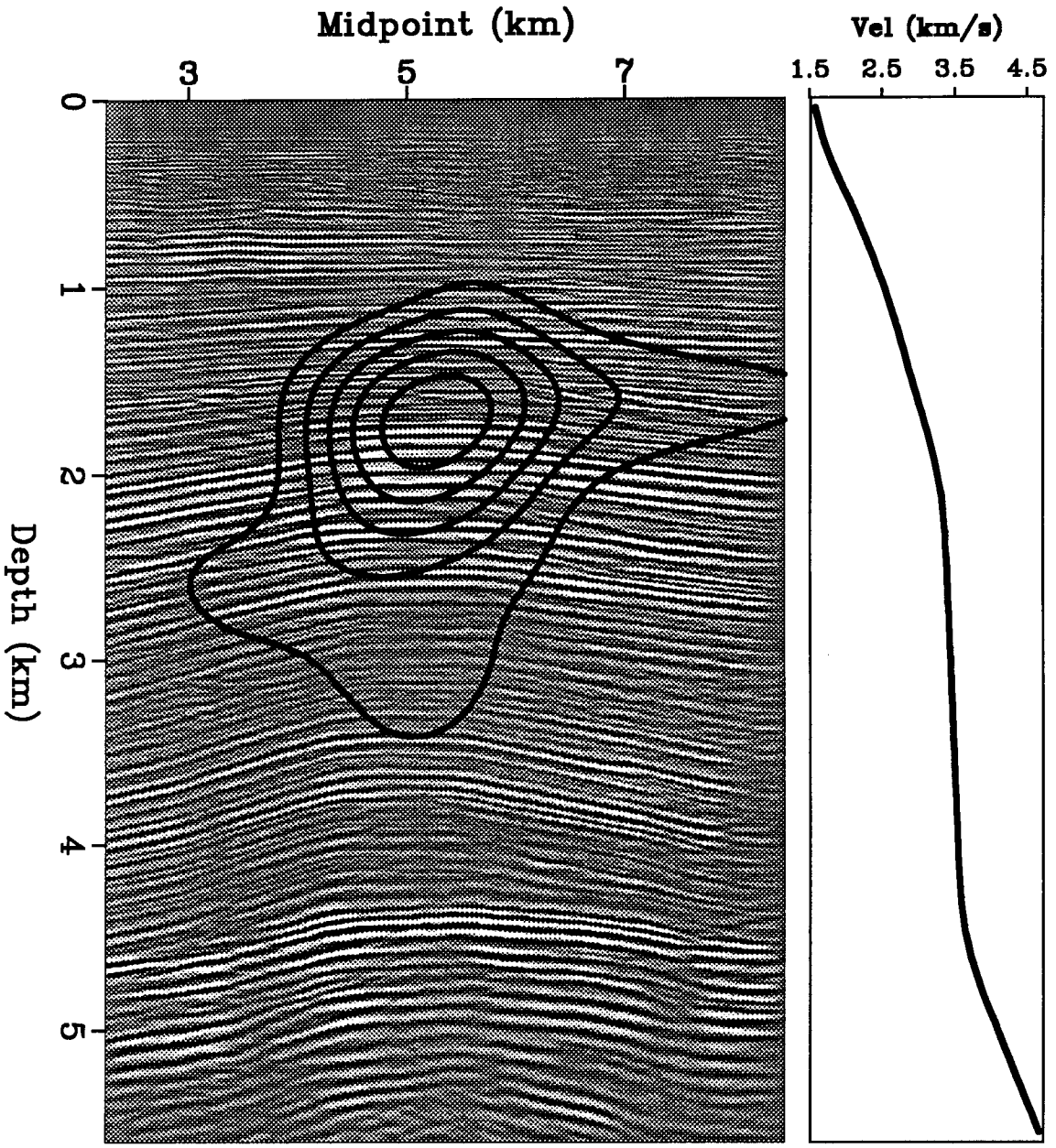

FIG. 4.6. The velocity model estimated with use of beam stacks is shown as the sum of two components: one background velocity profile and one anomalous function. The background velocity is plotted on the right, while the anomalous velocity is displayed with a contour plot superimposed onto the result of migrating the stacked data with the estimated velocity as a velocity function. The contour interval is -40 m/s.

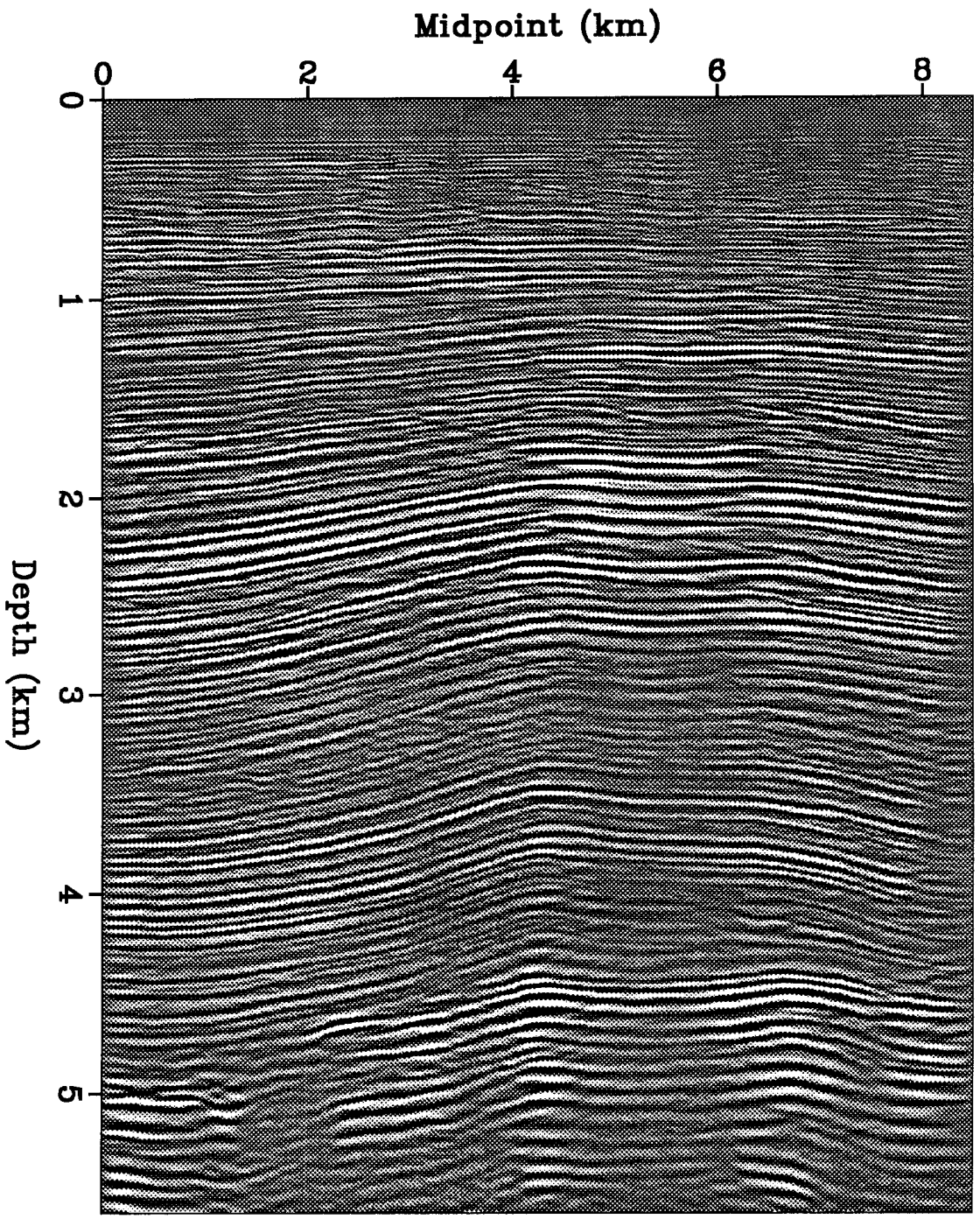

FIG. 4.7. The result of migrating the stacked data when the background velocity is used as a velocity function.

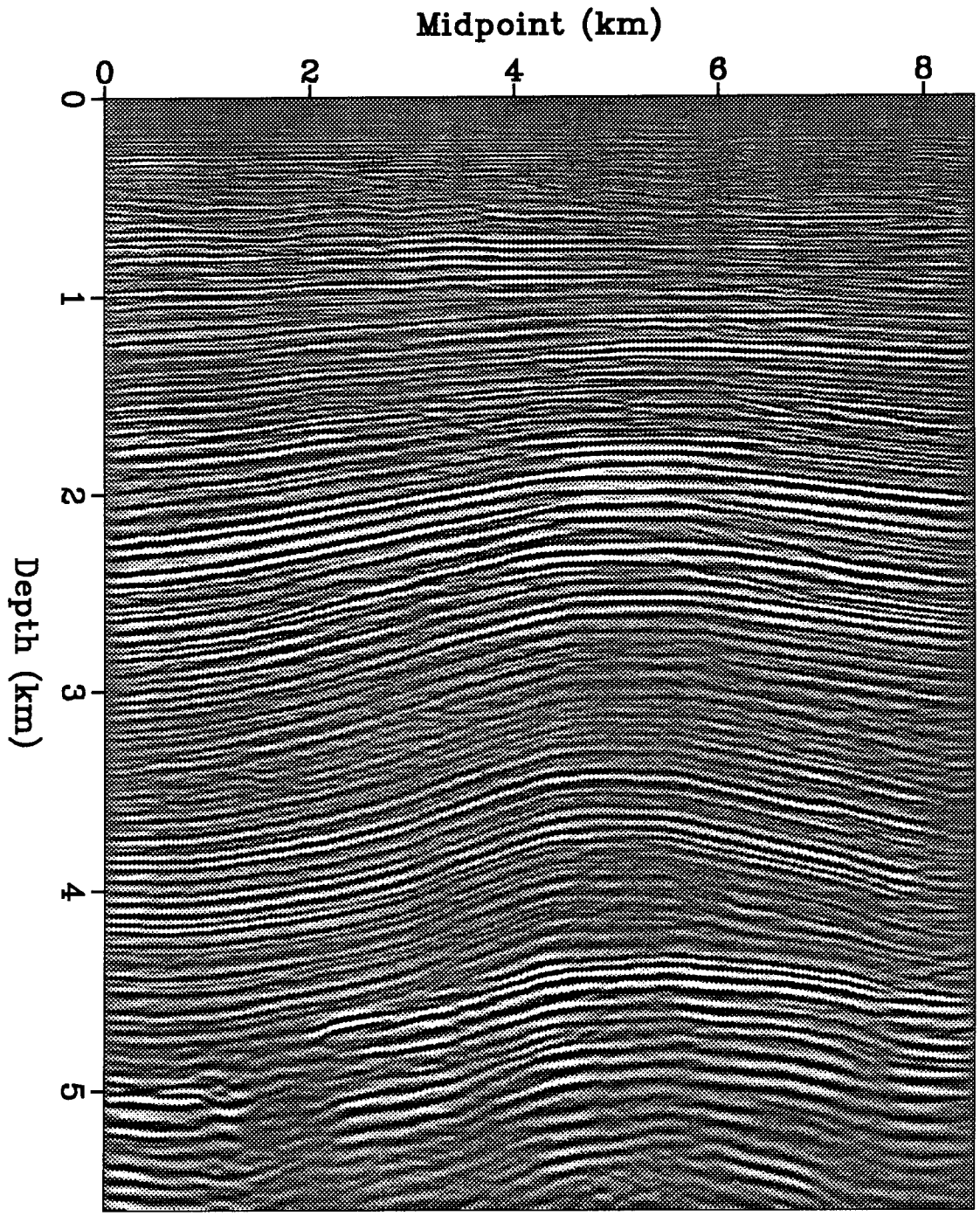

FIG. 4.8. The result of migrating the stacked data when the estimated velocity is used as a velocity function.

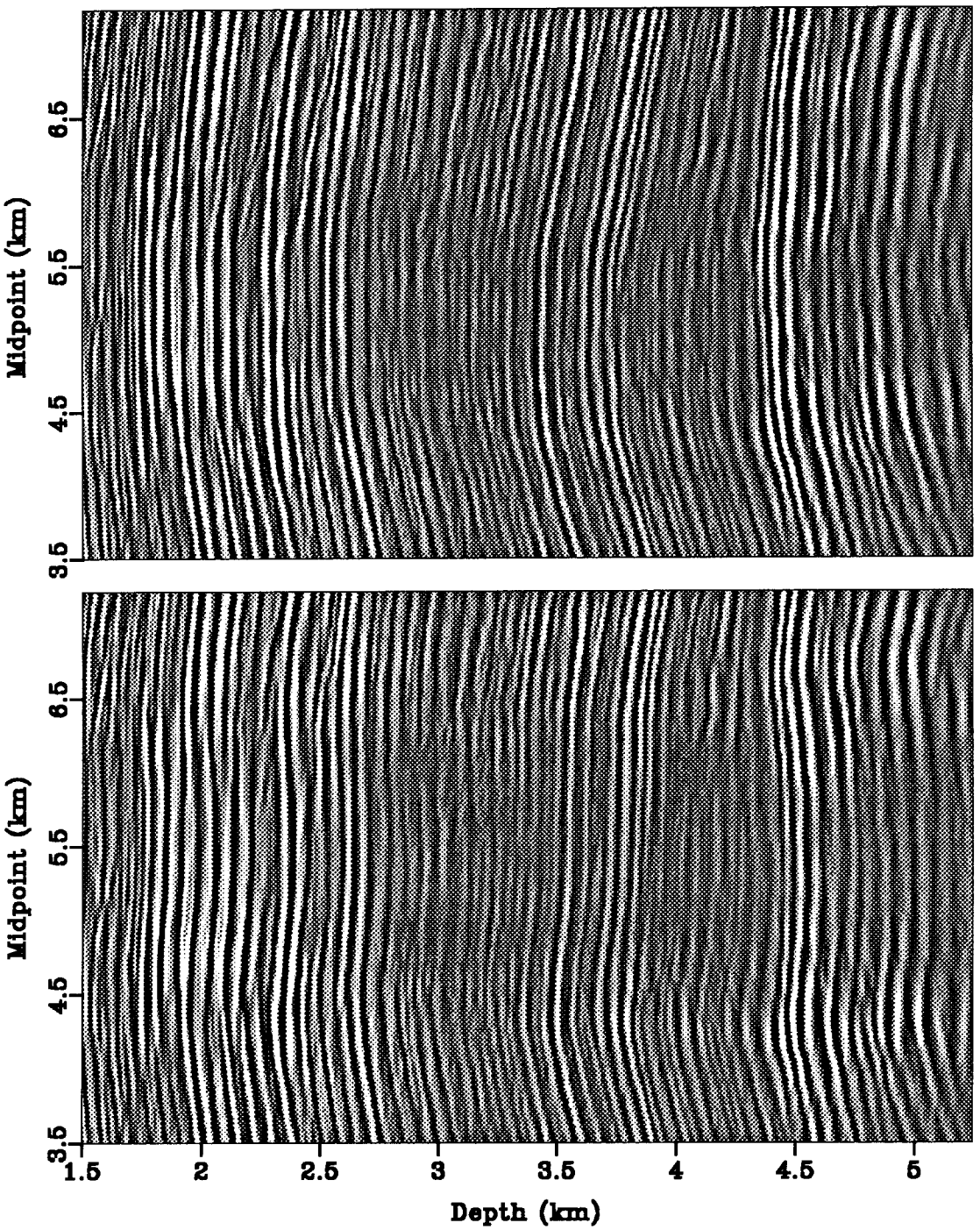

FIG. 4.9. The comparison of the migration results obtained when the background velocity (top) and the estimated velocity (bottom) are used as velocity functions. The estimated velocity correctly positions the top of the anticline and improves the focusing of the reflectors underneath the anomaly.

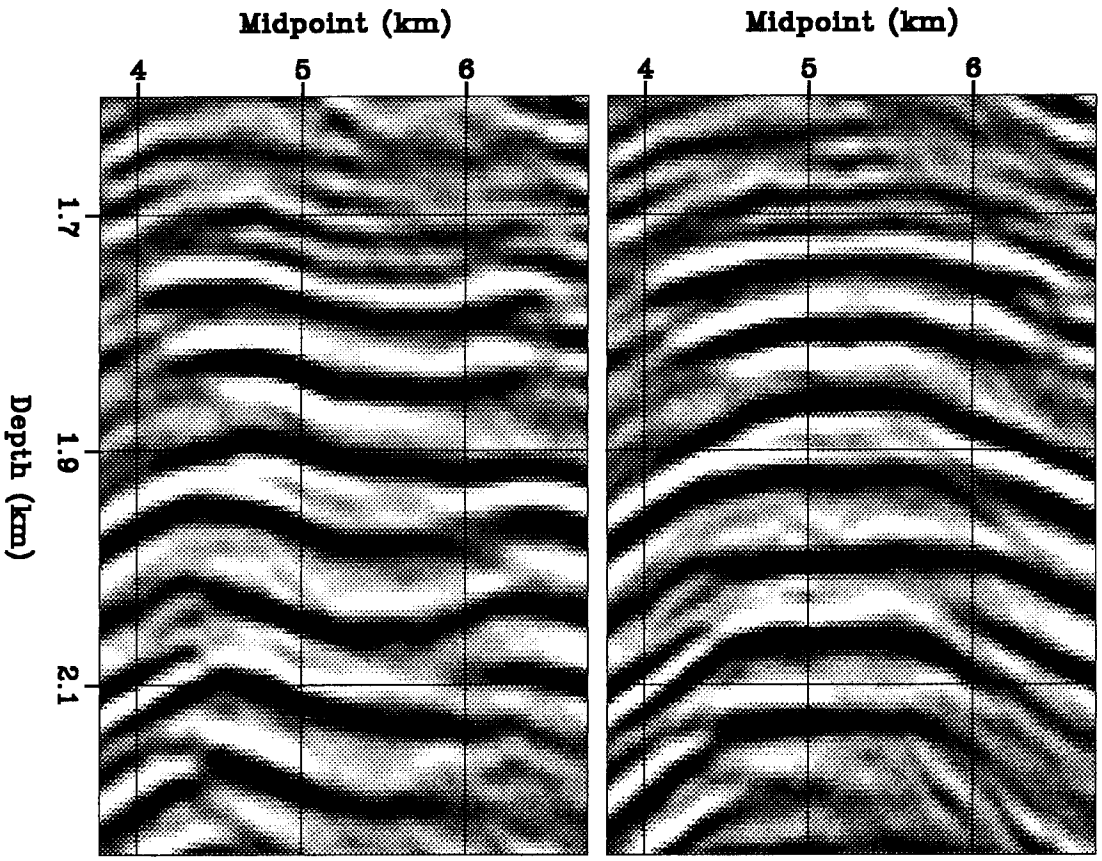

FIG. 4.10. The migrations of the top of the anticline using the background velocity (left) and the estimated velocity (right) as velocity functions. The horizontal reflectors located between the depths of 1.9 km and 2.2 km were probably caused by boundaries between the gas reservoirs and water tables.

Figure 4.10 compares the results of migrating the top of the anticline with the estimated velocity (left) and the background velocity (right). The upper reflectors of the anticline (from 1.7 km to 1.9 km) are clearly convex after migration with the estimated velocity, while the lower reflectors (from 1.9 km to 2.2 km) are flat at the top. These horizontal reflections were probably caused by the boundaries between the gas reservoirs and water tables. This interpretation for the flat reflectors is possible only after migrating the data with the estimated velocity model; it would not have been possible from the migration with the background velocity.

4.2.1 Using beam-stacked data to check the estimation results

When a velocity model to be used for depth migration is built, it is important that the prestack data be used to check the quality of the results. The beam-stacked data can be readily used for this purpose of quality check: the actual position of the semblance peaks in the beam-stacked data can be compared with the positions predicted by the estimated velocity model.

Figure 4.11 and Figure 4.12 show the same slices of the beam-stacked data shown in Figure 4.2 and Figure 4.3, but superimposed onto the data are the offsets curves predicted by the ray tracing. The estimated velocity function was assumed when these offset curves were computed. The peaks of the beam stacks are well predicted by the final results of the estimation.

In section 4.1.1 I showed that the non-hyperbolicity in the moveouts caused by the velocity anomaly can be measured by use of beam stack. Figure 4.13 demonstrates that the estimated velocity model approximately predicts these non-hyperbolic moveouts. This figure shows the beam stacks' semblance for two non-hyperbolic reflections (Figure 4.4 and Figure 4.5) as functions of offset and the offset ray parameter. The solid lines superimposed onto the semblance plots correspond to the estimated velocity function, while the dashed lines correspond to perfectly hyperbolic moveouts. The estimated velocity clearly predicts non-hyperbolic moveouts, although the predicted offset curves do not exactly follow the sharp variations in the offsets of the semblance peaks. The velocity model was too smooth for modeling such sharp perturbations in the data.

4.3 CONCLUSIONS

The velocity-estimation method presented in this thesis was successful in estimating a low-velocity anomaly from field data. When the estimated velocity model was used in depth migrating the data, the mispositioning of the reflectors caused by the anomaly was corrected, and the focusing of the result was improved.

The estimated velocity well explains the prestack data and, in particular, the beam-stacked data. An analysis of the beam-stacked data shows that beam stacks can be used for measuring non-hyperbolic moveouts of the reflections. The estimated velocity anomaly approximately predicts these non-hyperbolic moveouts.

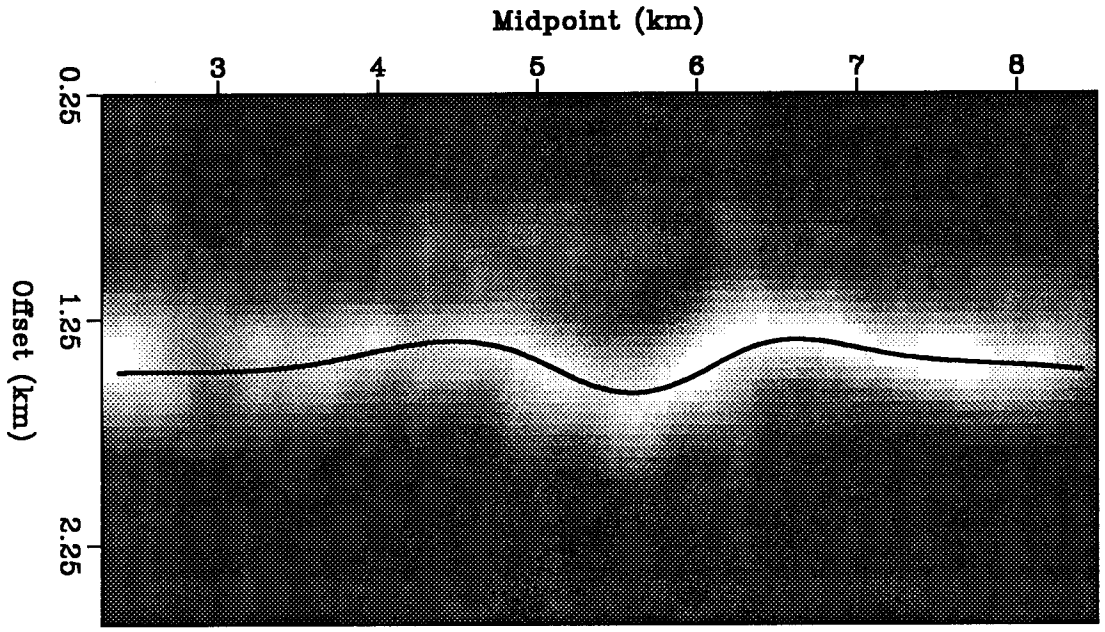

FIG. 4.11. Beam stacks' semblance as a function of offset and midpoint location, for the reflector at about 2 s in the stacked section shown in Figure 4.1. The black line superimposed onto the semblance plot corresponds to the beam stacks' offset predicted by the estimated velocity function.

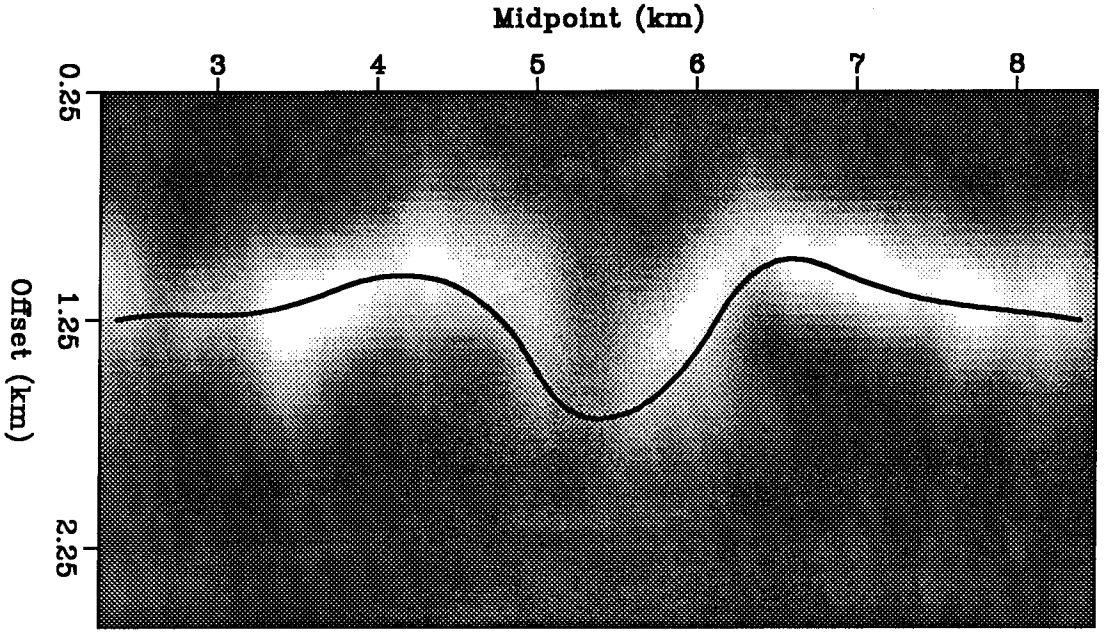

FIG. 4.12. Beam stacks' semblance as a function of offset and midpoint location, for the reflector at about 3.1 s in the stacked section shown in Figure 4.1. The black line superimposed onto the semblance plot corresponds to the beam stacks' offset predicted by the estimated velocity function.

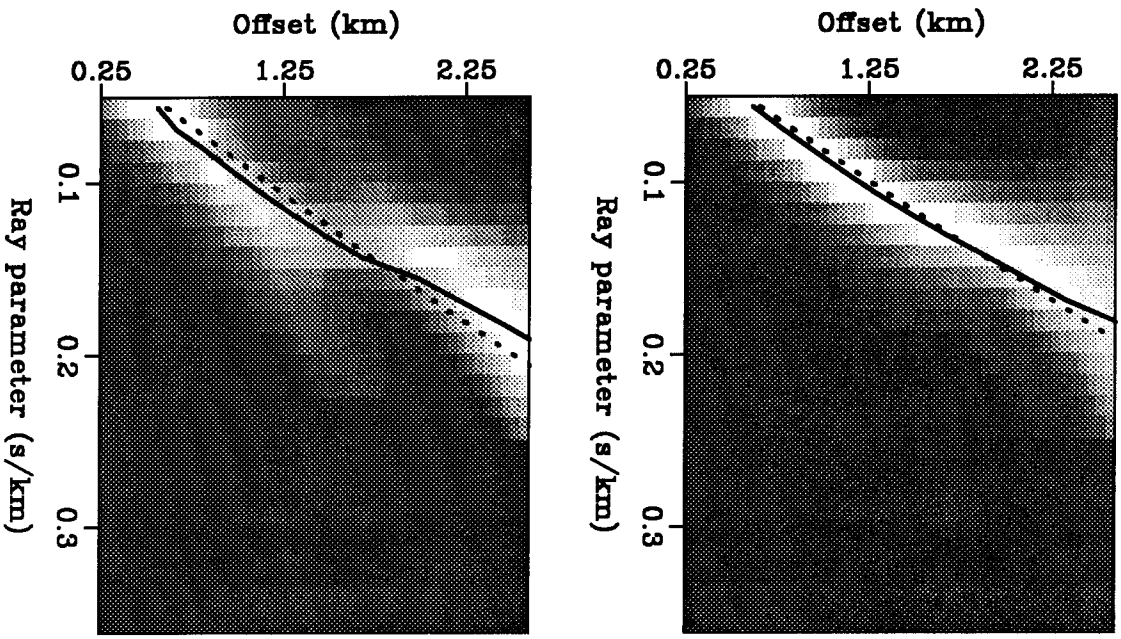

FIG. 4.13. Beam stacks' semblance for the non-hyperbolic reflection shown in Figures 4.4 and 4.5. The solid lines superimposed onto the semblance plots correspond to the estimated velocity function, while the dashed lines correspond to perfectly hyperbolic moveouts.